Eur. Phys. J. Spec. Top. (2026) 235:8397–8411
https://doi.org/10.1140/epjs/s11734-026-02368-x

THE EUROPEAN PHYSICAL JOURNAL SPECIAL TOPICS

Regular Article

Functional connectivity and long-range temporal correlations of neural activity in the alpha-range as markers of intellectual development in children

Alexander K. Kuc[a]

Plekhanov Russian University of Economics, Stremyanny Lane, 36, Moscow 115054, Russia

Received 2 April 2026 / Accepted 27 April 2026 / Published online 11 May 2026
© The Author(s), under exclusive licence to EDP Sciences, Springer-Verlag GmbH Germany, part of Springer Nature 2026

Abstract This study examined the dependence between neural dynamics, functional connectivity, and fluid intelligence in 90 children aged 8–14 years. Resting-state EEG was used to compute detrended fluctuation analysis (DFA), reflecting long-range temporal correlations, and phase-locking value (PLV), reflecting functional connectivity. Fluid intelligence was assessed with Raven's Progressive Matrices (RPM). DFA exponents in the right frontal alpha band correlated with RPM performance ($p = 0.04$). Alpha-band functional networks predicted individual RPM scores ($R = -0.32$, $p = 0.002$), and higher frontal DFA was associated with lower clustering in a negatively correlated network ($p = 1.9 \times 10^{-5}$). A classifier distinguished high and low performers with 76% accuracy ($F1\text{-score} = 0.8$, $p = 0.01$). These findings demonstrate that fluid intelligence in children is linked to both the temporal stability of alpha oscillations and functional network topology, which are interrelated. Combined DFA and PLV measures may serve as biomarkers of cognitive development.

1 Introduction

Childhood and early adolescence represent a critical period for the development of cognitive abilities that underlie academic achievement and future professional success [1]. Among these abilities, fluid intelligence occupies a central place, defined as the capacity to solve novel problems, identify patterns, and think abstractly, independently of previously acquired knowledge [2]. Understanding the neurophysiological mechanisms that support fluid intelligence during development is essential for both fundamental neuroscience and educational practice, as it may enable early identification of children at risk for cognitive difficulties and facilitate the development of targeted intervention programs [3].

One of the most widely used and validated tools for assessing fluid intelligence is Raven's Progressive Matrices (RPM) [4]. This non-verbal test requires participants to identify the missing element in a complex visual pattern, engaging cognitive processes such as logical reasoning, pattern recognition, and cognitive flexibility [5]. Owing to its minimal cultural and linguistic bias, RPM is particularly well-suited for studying intelligence across diverse populations, including children [6].

Electroencephalography offers a non-invasive and relatively inexpensive method for investigating the neural underpinnings of cognitive abilities in developing populations [7]. Over recent decades, a growing body of research has linked specific features of EEG oscillations to intellectual performance [8]. In particular, oscillations in the alpha range (approximately 8-13 Hz) are increasingly viewed not merely as markers of cortical idling, but as active mechanisms of top-down control [9–11]. According to the inhibition-timing hypothesis, alpha oscillations facilitate cognitive processing by selectively suppressing irrelevant neural activity, thereby directing information flow toward task-relevant regions [12]. This perspective was further developed in the concept of "gating by inhibition," which posits that alpha activity functionally blocks irrelevant pathways to optimize information processing [13].

Importantly, fluid intelligence is thought to arise not from the isolated functioning of individual brain regions, but rather from the dynamic interaction of distributed neural networks [14]. Functional connectivity, which quantifies the statistical dependence between neurophysiological signals recorded from different brain areas, provides

[a] e-mail: kuc1995@mail.ru (corresponding author)

valuable insight into these large-scale interactions [15]. The phase-locking value, a measure of the degree of phase synchronization between EEG signals, is widely used to assess functional connectivity in cognitive neuroscience [16]. Studies in both adults and children have demonstrated that individual differences in intelligence are associated with the topology of functional brain networks, particularly within the fronto-parietal system [17].

However, functional connectivity alone captures only one aspect of brain organization. An emerging line of research emphasizes the importance of the temporal structure of neural oscillations [18]. The brain is conceived as a complex system operating near a critical state, where an optimal balance between stability and flexibility is achieved [19]. One approach to quantifying this temporal structure is detrended fluctuation analysis (DFA), which measures long-range temporal correlations in the amplitude envelope of oscillatory activity [20]. Notably, DFA provides information that is statistically independent from traditional measures of spectral power and demonstrates high test-retest reliability, making it a promising biomarker for investigating individual differences in cognitive function [21].

Despite a growing body of evidence linking both functional connectivity and long-range temporal correlations to cognitive performance, these two families of measures are rarely integrated within a single study, particularly in children's samples. It remains unclear whether the temporal organization of alpha activity and the topology of functional brain networks are interrelated, and whether their combination yields greater predictive power for fluid intelligence in children.

To address this gap, the present study investigated the relationship between long-range temporal correlations (assessed using DFA), functional connectivity (assessed using PLV), and fluid intelligence (measured using RPM) in a sample of 90 children aged 8 to 14 years. We hypothesized that individual differences in RPM performance would be associated not only with the strength and topology of functional networks in the alpha band, but also with the temporal stability of alpha oscillations in frontal brain regions. Furthermore, we expected these two levels of analysis to be interrelated. To test these hypotheses, we recorded resting-state EEG, computed DFA and PLV across multiple frequency bands, performed correlation analyses with behavioral data, applied connectome-based predictive modeling (CPM), and trained a machine learning classifier to distinguish children with high and low RPM scores based on the identified neurophysiological markers.

2 Methods

2.1 Participants

A total of 90 schoolchildren, aged between 8 and 14 years old (41 females and 49 males), participated in the study. All children were in grades 3, 4, 5 and 7 at the same school. All participants were conditionally healthy and had no history of neurological disorders. None of the subjects had previously participated in similar studies.

All subjects participated in the experiment of their own volition, but only after obtaining the approval of their parents. Parents were informed about the aims and methods of the study, were able to ask any related questions and received detailed answers. In this way, parents were provided with all the necessary information to decide whether they approved of their child's participation in the study. Following this, parents signed an informed consent form.

This study was conducted according to the guidelines of the Declaration of Helsinki and approved by the Ethic Commitee of Immanuel Kant Baltic Federal University (protocol No. 32 of 04.07.2022).

2.2 Experimental procedure

The experimental study consisted of three main stages: a two-minute electroencephalogram (EEG) recording conducted in a resting state, testing using Raven's progressive matrices (RPM) to assess cognitive functions and performance of experimental tasks designed to assess basic cognitive abilities.

The RPM is a standardised non-verbal test that is widely used to assess cognitive abilities such as intelligence and abstract thinking ability [4]. This test is considered as an indicator of fluid intelligence, defined as the ability to solve novel logical problems without prior learning [22]. Fluid intelligence is characterised by the following cognitive skills:

- abstract thinking—the ability to find logical connections between elements, to operate with symbols and concepts outside of a specific context [23];
- logical thinking—the ability to draw deductive and inductive conclusions, to find a general principle on the basis of particular cases [24];
- problem solving—ability to formulate hypotheses, build mental models to find solutions [25];
- pattern detection—identifying hidden rules and structures in presented visual patterns [4];
- cognitive flexibility—the ability to adapt to new conditions, to switch between different strategies when solving tasks [26].

The RPM test comprises 60 multiple-choice questions divided into 5 blocks of increasing difficulty. Each task represents a visual stimulus—a pattern consisting of dots, lines and figures, in which one element is missing. The task of the subject is to select the correct element from the proposed variants, which logically completes the pattern.

To assess basic cognitive abilities, we introduced experimental tasks that are closely related to different types of cognitive activity in the learning process [27], namely:

- visual search is the person's ability to efficiently find specific visual information among a complex set of stimuli. It plays a key role in tasks requiring visual attention, pattern recognition and information retrieval;
- working memory is an integral part of the temporary storage and manipulation of information during cognitive tasks. It affects a person's ability to process and retain data, especially when performing tasks involving multitasking, problem solving and decision making;
- mental arithmetic focuses on a person's numerical processing abilities, including mental calculation, mathematical reasoning and quantitative problem solving. Knowledge of mental arithmetic is necessary to solve a wide range of academic and practical tasks;
- the ability to combine cognitive abilities is crucial because almost any complex cognitive task can be decomposed into several simple ones. Thus, the ability to solve such a complex task will be determined, in particular, by the effectiveness of combining different cognitive abilities.

To ensure maximum comfort of the participants and to reduce possible stress, the EEG recording was conducted in a familiar environment for the subjects. The use of a mobile EEG recorder minimised the limitations of the participant's movement. The EEG recording were conducted at the educational facility in the morning in a room with natural light.

External stimuli such as loud sounds, extraneous noises and harsh lightning were minimised. Participants were in comfortable chairs and sat with their eyes open, maintaining a relaxed state. Before staring the recording, subjects were given detailed instructions to remain still and remain calm throughout the procedure.

2.3 EEG recording and preprocessing

EEG signals were recorded using "LiveAmp" device (Brain Products, Germany) with Ag/AgCl ActiCap active electrodes. A total of $C = 64$ channels were recorded in accordance with the "10-10" system [28], with ground and reference electrodes positioned at the "Fpz" and "Fz" positions, respectively. Prior to the commencement of data acquisition, the scalp was treated with "NuPrep" abrasive gel to enhance skin conductivity. Additionally, "SuperVisc" conductive gel was applied during electrode placement to attain optimal impedance values. Prior to the commencement of the experiment, the impedances were verified to ensure that the desired value of $< 25k\Omega$ was achieved.

EEG signals were recorded at a sampling rate of 1000 Hz and subsequently processed using a series of filters. These comprised a band-pass filter with cut-off points of 1 Hz and 100 Hz, and a 50 Hz notch filter. The removal of physiological artefacts related to heart rate and eye movements was achieved through the utilisation of independent component analysis (ICA) [29]. ICA was implemented using the Fieldtrip toolbox for Matlab [30]. The EEG dataset, comprising 64 channels, was then decomposed into 64 independent components. The components that contained artefacts were then identified and removed, and the EEG signals were reconstructed [31].

2.4 Detrended fluctuation analysis

Detrended fluctuation analysis (DFA) is a powerful tool for the analysis of complex time series, especially when the objective is to comprehend the structure of data at different time scales and to identify latent correlations and trends [32, 33].

The results of DFA is the scaling factor (μ), which characterises the type of correlation present in the data [34]. For example, $\mu \sim 0.5$ indicates the absence of correlations, which corresponds to a random wandering process or white noise; $\mu < 0.5$ indicates an anticorrelated process; $\mu > 0.5$ indicates the presence of long-range correlations, which may indicate a stable trend.

The DFA characteristic was calculated in 4 frequency ranges $[f_1, f_2]$ corresponding to the main brain rhythms: the delta- and theta-ranges (1–7 Hz) reflecting low-frequency activity; the alpha-range (6–13 Hz); the beta1-range (13–20 Hz); and the beta2-range (20–30 Hz). The DFA was calculated for each EEG channel ($i = 1, ..., C$, $C = 64$) in each of four frequency ranges.

The selection of frequency band boundaries accounted for the developmental characteristics of the sample. Specifically, the alpha range was defined as 6–13 Hz rather than the conventional 8–13 Hz used in adult studies. This extended lower boundary accommodates the individual peak of the alpha rhythm, which in children aged 8–14 years often shifts toward lower frequencies (the so-called "child alpha" or low-alpha component). The lower

limit of 6 Hz ensures that task-relevant oscillatory activity is not excluded, while the upper limit of 7 Hz for the delta/theta band prevents overlap with the alpha range. This frequency partitioning is consistent with previous developmental EEG studies [35].

The DFA-based analysis of each i-th EEG signal $X_i(t)$ consisted of the following steps:

1. **Filtering of the signal $X_i(t)$ in the frequency range** $[f_1, f_2]$. For this purpose, we used the filter with finite impulse response (FIR), the order of which was set to $2/f_1$ s, where f_1 denotes the lower frequency of the analysed frequency range. This guarantees that the filter window covers at least two cycles of oscillations with frequency f_1 Hz.
2. **Computation of the amplitude envelope using the Hilbert transform.** The Hilbert transform $\hat{X}_i(t)$ is applied to the filtered signal $X_{i,\Delta f}(t)$ to obtain the phase-shifted signal:

$$\hat{X}_i(t) = \frac{1}{\pi}\int_{-\infty}^{\infty} \frac{X_{i,\Delta f}(\tau)}{t-\tau} d\tau. \tag{1}$$

The analytical signal $Z_i(t)$ is obtained as the sum of the original signal and its Hilbert transform: $Z_i(t) = X_{t,\Delta f}(t) + j\hat{X}_i(t)$, where j is an imaginary unit. The amplitude envelope is defined as the modulus of the analytical signal:

$$A_i(t) = |Z_i(t)| = \sqrt{X_{i,\Delta f}(t)^2 + \hat{X}_i(t)^2}. \tag{2}$$

3. **Construction of the cumulative profile of the signal.** A cumulative profile, denotes as $Y_i(k)$, is constructed from the amplitude envelope $A_i(t)$ of length N:

$$Y_i(k) = \sum_{t=1}^{k} \left[A_i(t) - \bar{A}_i\right], \tag{3}$$

where $\bar{A}_i = \frac{1}{N}\sum_{t=1}^{N} A_i(t)$.
4. **Dividing the dataset into discrete segments.** The cumulative profile is partitioned into $N_s = N/s$ segments of length s with 50% overlap.
5. **Removal of the trend observed in each segment.** Polynomial regression is performed in each segment of length s. The resulting trend $Y_i^s(k)$ is subtracted from the aggregate series, obtaining "decorrelated" fluctuations:

$$F_i^2(s, \upsilon) = \frac{1}{s}\sum_{k=1}^{s} (Y_i[(\upsilon-1)s + k] - Y_i^s(k))^2, \tag{4}$$

where $\upsilon = 1, 2, ..., N_s$ is the segment index.
6. **Calculation RMS fluctuation.** The standard deviation was calculated for each segment:

$$F_i(s) = \sqrt{\frac{1}{N_s}\sum_{\upsilon=1}^{N_s} F_i^2(s, \upsilon)}. \tag{5}$$

7. **Repetition of calculations for different scales.** Steps 3-5 are repeated for different values of s, which correspond to different scales.
8. **Construction of the dependence and estimation of the scaling factor.** The function $F(s)$ is plotted on a logarithmic scale. In case the time series has a self-similar structure, the dependence will have the form of a straight line:

$$F_i(s) \sim s^{\mu^i_{\Delta f}}. \tag{6}$$

The exponent $\mu^i_{\Delta f}$ (scaling factor) is estimated by calculating the slope o the line on a logarithmic scale.

The DFA exponent was calculated using the Neurophysiological Biomarker Toolbox package (NBT, http://www.nbtwiki.net/) for Matlab. The DFA exponent was calculated on 30-s trials using windows s from 2 to 15 s. The lower bound of 2 s ensures that the analysis is not contaminated by high-frequency noise and allows a sufficient

number of data points per window for reliable fluctuation estimation. The upper bound of 15 s was determined by two factors: first, the standard recommendation that the maximum window size should not exceed half of the signal length ($s_{\max} \leq N/2$), which for a 30-s trial yields 15 s [20]; second, this upper limit corresponds to a frequency of approximately 0.07 Hz, capturing slow neurodynamic processes related to sustained attention and arousal without violating signal stationarity assumptions.

Despite its widespread applicability, DFA has several methodological constraints that should be considered when interpreting the results. First, DFA is sensitive to non-stationarities and external trends in the signal, which can lead to spurious estimates of the scaling exponent if not properly removed [36]. To mitigate this, we applied detrending within each window (Step 5 in the algorithm above) and carefully screened the data for artefacts prior to analysis. Second, reliable estimation of the DFA exponent requires sufficiently long time series; in the present study, the use of 30-s epochs with window sizes up to 15 s meets the minimum recommendations for robust estimation. Third, the interpretation of the scaling exponent can be ambiguous in signals that arise from a mixture of different physiological processes, as the observed scaling may reflect a superposition of multiple underlying mechanisms rather than a single scale-free process. Nevertheless, with appropriate preprocessing and standardized protocols, DFA remains a valuable tool for characterizing long-range temporal correlations in neural oscillations.

2.5 Statistical testing

A permutation correlation test with cluster correction was performed to identify associations between DFA exponents and various human cognitive states.

The cluster permutation correlation test is a statistical method that has gained significant traction in the field of cognitive neuroscience [37]. It is employed to identify significant correlations between neurophysiological data and behavioural indicators in multiple comparisons. A key strength of this method is its ability to account for spatial, temporal, or frequency dependence of the data. This feature serves to reduce the probability of false positives, thereby enhancing the reliability and precision of the results obtained.

For each data point, the correlation between the neurophysiological metric (DFA exponent) and behavioural measures was calculated using Pearson or Spearman correlation, depending on the normality of the data distribution [38]. The identification of significant points was based on a threshold level of significance. Spatially adjacent points were then grouped into clusters based on a predefined criterion (number of neighbouring elements and proximity of EEG channels). For each cluster, statistics were calculated as the sum of the values of the statistical criterion within the cluster. Subsequently, behavioural measures were randomly allocated between subject, and the correlation calculation, cluster formation and calculation of their statistics were performed once more. This process was repeated many times. The resulting empirical distributions of cluster statistics were then compared to the proportion of permutations in which the statistics of random clusters equalled or exceeded the statistics of the observed cluster.

The implementation of cluster permutation correlation testing was conducted utilising the Fieldtrip package for Matlab [30]. The statistical analysis was conducted employing Pearson's correlation coefficient. Monte Carlo test with 1000 permutations was used as a computational method. The cluster approach, which involved maximising the sum of t-values within the cluster, was utilised to address the issue of multiple comparisons. The significance level for cluster formation was set at 0.05. The minimum number of neighbouring elements required for cluster formation was 2. The list of neighbouring electrodes was generated by triangulation method based on channel topography. Behavioural characteristics corresponding to different cognitive states (the result of passing Raven's progressive matrices, the efficiency of performing experimental tasks, namely reaction time and correctness) were used as an independent variable.

2.6 Phase coherence

PLV (phase locking value) characteristic was utilised to evaluate phase synchronisation between EEG channels. PLV is a metric of phase synchronisation of neurophysiological signals employed to assess functional connectivity between disparate brain regions based on their electrical activity [39]. This method is extensively employed in studies based on electroencephalography and magnetoencephalography to analyse between-regional interactions, including the study of cognitive processes [40].

PLV is a measure of the degree of phase coherence between two time series of signals, $x(t)$ and $y(t)$, recorded from different electrodes. For each time point, the phase difference between the signals is calculated:

$$\Delta(t) = \phi_x(t) - \phi_y(t), \tag{7}$$

where $\phi_x(t)$ and $\phi_y(t)$ are the instantaneous phases of the signals extracted using the wavelet transform.

PLV is defined as the modulus of the mean of the complex exponents of the phase difference:

$$\mathrm{PLV} = \left| \frac{1}{N} \sum_{t=1}^{N} e^{i\Delta\phi(t)} \right|, \tag{8}$$

where N is the number of time points. The PLV value varies from 0 (complete absence of phase synchronisation) to 1 (complete phase synchronisation).

The calculation of PLV was performed by filtering the EEG signals on each channel with an FIR filter across four frequency ranges corresponding to the main brain rhythms: delta- and theta-ranges (1–7 Hz), reflecting low-frequency activity; alpha-range (6–13 Hz); beta1-range (13–20 Hz); beta2-range (20–30 Hz). PLV values were calculated on 30-s segments recorded at rest.

2.7 Connectome-based predictive modelling

Connectome-based Predictive Modelling (CPM) was utilised to predict individual behavioural performance based on functional brain connectivity [41]. This approach applies functional or structural brain connectivity matrices in conjunction with behavioural metrics to construct a predictive model. Subsequent to this, the significance of the model is tested using cross-validation and permutation tests.

The functional connectivity between brain regions was determined using PLV values represented as an $M \times M$ connectivity matrix, where M is the number of EEG channels (nodes).The matrix values thus represented the strength of connectivity between nodes.

Each connection (edge) of the connectivity matrix was tested for correlation with a behavioural measure, namely the performance of Raven's progressive matrices, using Pearson correlation. Significant relationships were selected using a threshold of $p < 0.05$.

The total metrics were calculated by summing the values of significant correlations for each subject. Separate metrics were defined for positive and negative correlations.

In the next step, a linear regression model was constructed:

$$y = \beta_0 + \beta_1 X, \tag{9}$$

where y is the behavioural metric (the result of performing Raven's progressive matrices) and X is the total connectivity metric.

Leave-One-Out Cross-Validation (LOOCV) was used to evaluate the effectiveness of the model. The evaluation of the model was conducted on data that was not involved in its training.

Permutation testing was used to testing the significance of the predictions. Behavioural metrics were randomly shuffled between subjects, and for each permutation the correlations between predicted and true values were recalculated. The number of permutations was set at 1000.

The results were then visualised using circle plots, allowing the results to be compared to brain regions.

2.8 Network measures

The following metrics were calculated for functional networks showing correlation with behavioural characteristics:

Clustering coefficient

The clustering coefficient is a metric that quantifies the degree of connectivity between neighbouring nodes in a network. For node i, the local clustering coefficient is calculated as:

$$C_i = \frac{1}{k_i(k_i - 1)} \sum_{j,k} (A_{ij} A_{ik} A_{jk})^{1/3}, \tag{10}$$

where A_{ij} is the element of the adjacency matrix, k_i is the degree of node i (the number of its neighbours).

The global clustering coefficient is calculated as the average value of C_i over all nodes:

$$C = \frac{1}{N} \sum_{i=1}^{N} C_i. \tag{11}$$

Global efficiency

Global efficiency reflects how efficiently information spreads through the network. Global efficiency was defined as the average of the inverse distances between all pairs of nodes:

$$E_{\text{global}} = \frac{1}{N(N-1)} \sum_{i \neq j} \frac{1}{d_{ij}}, \tag{12}$$

where d_{ij} is the shortest distance between nodes i and j.

Strength

The node strength was calculated as the sum of the weights of its links:

$$S_i = \sum_j A_{ij}. \tag{13}$$

The global strength of the network was defined as the average of the strength of all nodes:

$$S = \frac{1}{N} \sum_{i=1}^{N} S_i. \tag{14}$$

2.9 ML-based classifier

A classifier was applied in order to categorise subjects according to their performance in completing Raven's progressive matrices. For this purpose, subjects were divided into two classes based on the median value of the score assigned after passing the Raven's progressive matrices. The classifier was trained using a set of features that demonstrated a statistically significant correlation with behavioural performance.

The training process incorporated an SVM (Support Vector Machine) classifier with a linear kernel. The linear SVM objective is to ascertain the optimal hyperplane that will enable efficient separation of the two classes in the feature space, maximising the margin between the data points of each class. This approach increases the robustness of the model to noise and improves the generalisability. The regularisation parameter, denotes as R, functions as a hyperparameter, achieving a balance between maximising the margin and minimising the classification error. The GridSearch method was used to optimise this hyperparameter. The objective of this hyperparameter optimisation was to maximise the $F1$-score [42].

The performance of the model was evaluated through the utilisation of k-fold cross-validation. Data from all subjects were divided into $k = 10$ subsets. The model was trained on $k - 1$ subset and evaluated on the remaining subset. This process was repeated 5 times.

In order to evaluate the quality of the model, the following metrics were calculated based on the number of true positive (TP), true negative (TN), false positive (FP) and false negative (FN) results:

Accuracy. The proportion of objects for which the model correctly predicted the class:

$$\text{Accuracy} = \frac{\text{TP} + \text{TN}}{\text{TP} + \text{TN} + \text{FP} + \text{FN}}. \tag{15}$$

Recall. The proportion of correctly found positive objects among all objects of positive class:

$$\text{Recall} = \frac{\text{TP}}{\text{TP} + \text{FN}}. \tag{16}$$

Precision. The proportion of correctly predicted positive objects among all objects predicted as a positive class:

$$\text{Precision} = \frac{\text{TP}}{\text{TP} + \text{FP}}. \tag{17}$$

F1-score. Harmonic mean between precision and recall:

$$F1\text{-score} = 2 \times \frac{\text{Precision} \times \text{Recall}}{\text{Precision} + \text{Recall}}. \tag{18}$$

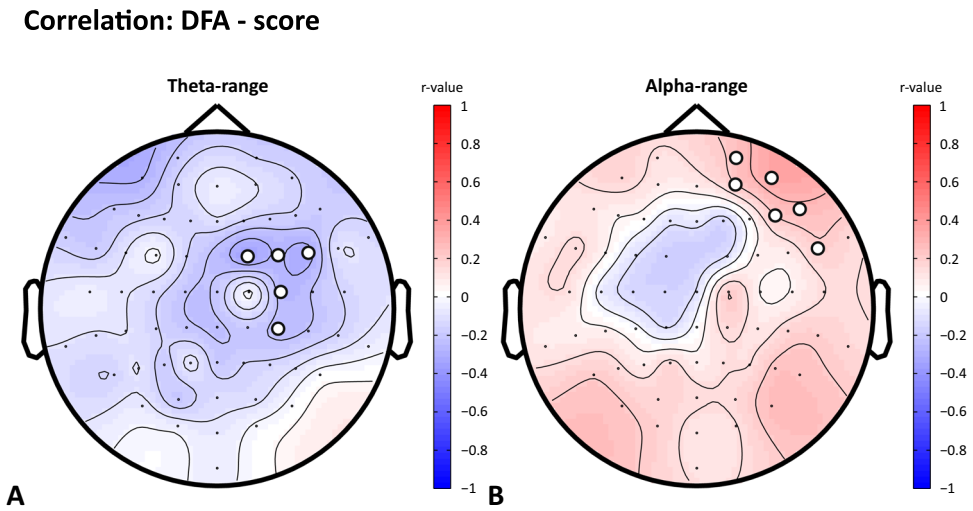


Fig. 1 Statistically significant correlation clusters were revealed by analysing the relationship between the DFA exponent calculated for each EEG channel in the theta- (**A**) and alpha- (**B**) ranges and the result of Raven's progressive matrices. The side panels illustrate the Pearson correlation coefficient. EEG channels demonstrating significant correlations were grouped into positive and negative clusters and marked with white circles

3 Results

3.1 Results of correlation of DFA with behavioural results

After performing cluster permutation correlation testing between the DFA exponent and the Raven's Progressive Matrices result, two statistically significant clusters were identified. The first cluster with $p = 0.04$ was identified in the theta-range and was located in the central and central-parietal regions of the brain predominantly in the right hemisphere (Fig. 1A). The second cluster with $p = 0.04$ was detected in the alpha-range and was located in the right frontal region of the brain (Fig. 1B).

After performing cluster permutation correlation testing between DFA exponent and experimental task performance, the following results were obtained.

Analysis of the dependence of the DFA exponent and correctness of mental arithmetic task performance revealed two statistically significant clusters. The first cluster with $p = 0.005$ was detected in the alpha-range and was located in frontal, frontal-central, central and right temporal brain regions (Fig. 2A). The second cluster with $p = 0.02$ was detected in the beta1-range and was located in central and frontal-central brain regions predominantly in the right hemisphere (Fig 2B).

Analysis of the relationship between the DFA exponent and reaction time during the visual search tasks revealed one statistically significant cluster with $p = 0.03$ in the alpha-range. This cluster was located in the occipital and parietal regions of the brain (Fig. 2C).

Analysis of the dependence of the DFA exponent and correctness of performance on the combined function tasks revealed two statistically significant clusters. The first cluster with $p = 0.01$ was identified in the alpha-range and was located in the right frontal. frontal-central and central regions of the brain (Fig. 2D). The second cluster with $p = 0.01$ was detected in the beta1-range and was located predominantly in the right frontal-central, right central and parietal brain regions (Fig. 2E).

3.2 Results of correlation of PLV with behavioural results

An analysis was then performed to discover functional networks that could predict subject's behavioural performance reflecting different human cognitive states, namely the performance of Raven's progressive matrices, as well as the performance of experimental tasks (reaction time and correctness of mental arithmetic, visual search, working memory and combined functions). For each subject, functional brain networks were constructed by calculating the PLV characteristic between each of the 64 EEG channels in four frequency ranges (delta+theta, alpha, beta1 and beta2). Correlations between all functional connectivity and behavioural performance with a statistical threshold of $p < 0.05$ were used to identify functional connectivity that had a statistically significant relationship with behavioural performance in each frequency ranges. To determine which of these networks had predictive potential, the connectome-based predictive modelling (CPM) method was used, in which Leave-One-Out Cross-Validation (LOOCV) was performed to build and test predictive models.

The analysis revealed that only the alpha-range contains a network positively correlated with the performance of Raven's progressive matrices, consisting of 28 edges, and negatively correlated with the performance of Raven's progressive matrices, consisting of 29 edges. The strength of the predictive model was evaluated by assessing the statistical significance of the relationship between the observed and the model-predicted outcome of performing

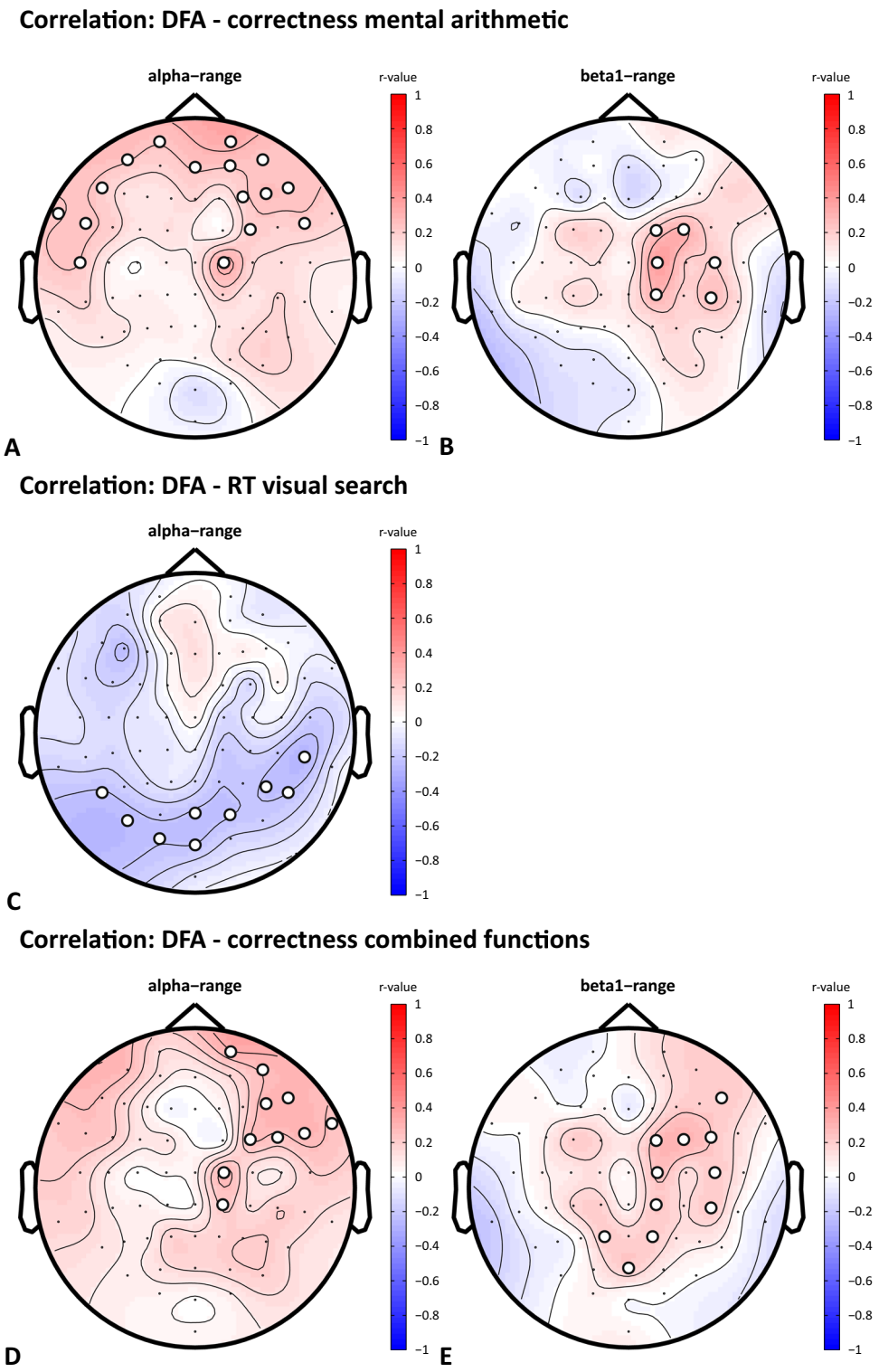


Fig. 2 Statistically significant correlation clusters were identified when analysing the relationship between the DFA exponent calculated for each EEG channel and performance on the experimental tasks. The side panels illustrate the Pearson correlation coefficient. EEG channels demonstrating significant correlations were grouped into positive and negative clusters and marked with white circles

Raven's progressive matrices. The results showed that the combination of both networks could reliably predict the actual results of performing Raven's progressive matrices ($R = -0.32$, $p = 0.002$) (Fig. 3).

Figure 4 visualise networks that are positively and negatively correlated with results of Raven's progressive matrices. The network that positively correlates with the results of Raven's progressive matrices includes two subnetworks localised separately in the right and left cerebral hemispheres and demonstrates functional connections between occipital and frontal regions (Fig. 4A).

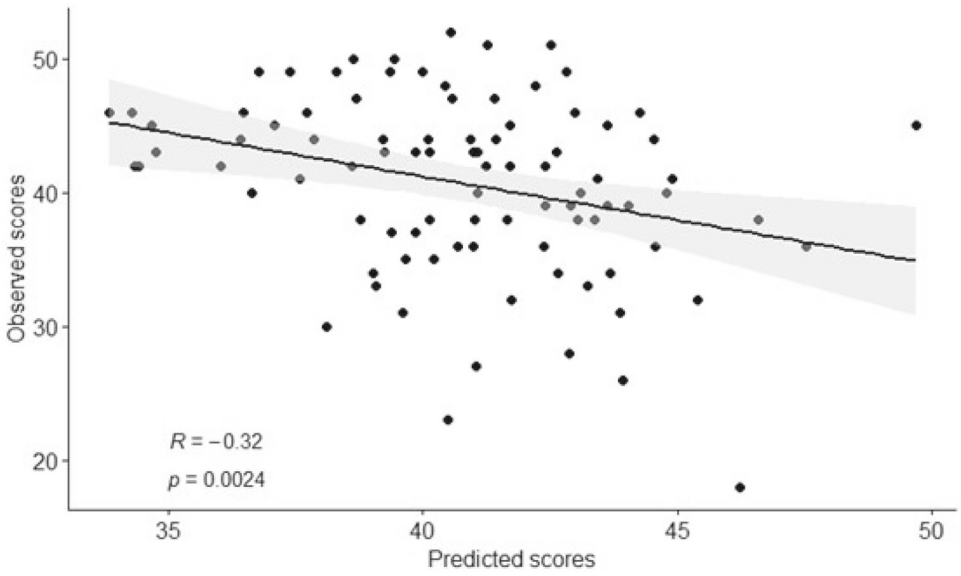


Fig. 3 Validation of the CPM model. The relationship between the observed and predicted results of the Raven's progressive matrices in Leave-One-Out Cross-validation

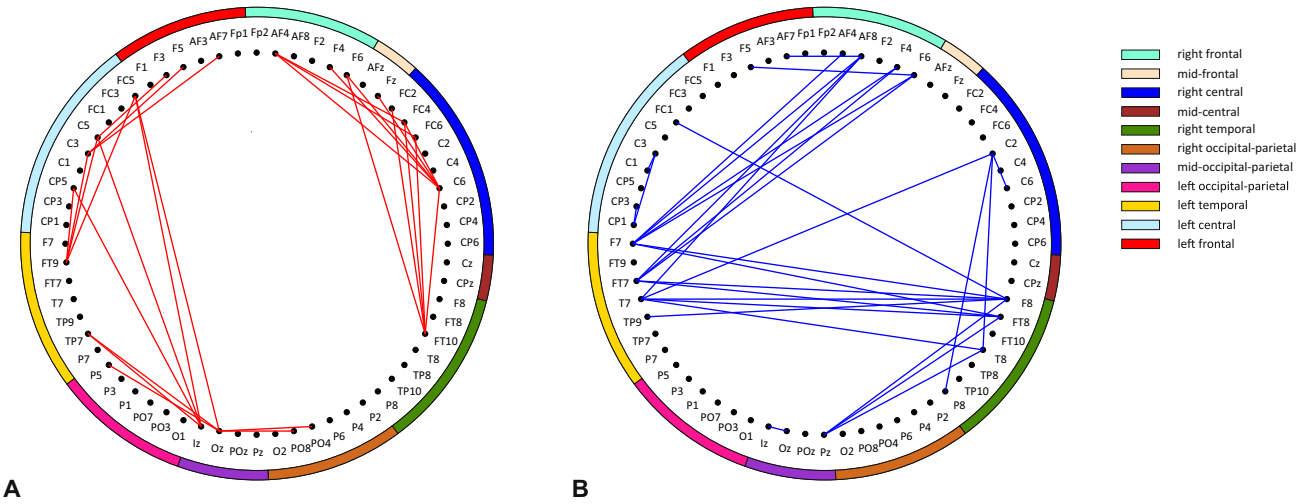


Fig. 4 Visualisation of the network positively and negatively correlated with results of Raven's progressive matrices in the form of the circle plot: nodes are located on a circle roughly reflecting brain anatomy and are colour coded according to brain regions. Functional relationships showing positive correlations are marked with red lines. Functional relationship showing negative correlations are marked with blue lines

The network negatively correlated with the results of Raven's progressive matrices demonstrates functional connectivity between 3 brain regions: right frontal, left temporal and right temporal (Fig. 4B).

3.3 Results of correlation of DFA with network measures

Since networks correlating with behavioural characteristics, namely the outcome of performing Raven's progressive matrices, were identified only in the alpha-range, we looked at whether the DFA exponents in the right frontal region of the brain (Fig. 1B) correlate with the network metrics. To do this, we calculated the following metrics for both the network positively correlated and the network negatively correlated with the results of performing Raven's progressive matrices: clustering coefficient, global efficiency and node strength.

We calculated the correlation coefficient between each metric of the positive and negative network and the DFA exponent averaged over the cluster channels in the right frontal region of the brain. The result showed that only the clustering coefficient for the negative network was significantly correlated with the DFA exponent in the alpha range ($p = 1.9e-05$, $R = -0.44$). The correlation results of the network metrics are presented in Table 1.

Table 1 Results of correlation analysis of network metrics and DFA exponent in the alpha range of the frontal region

	Positive network	Negative network
Clustering coefficient	$p = 0.58$, $R = -0.059$	**p = 1.9e–05, R = − 0.44**
Global efficiency	$p = 0.99$, $R = -0.001$	$p = 0.07$, $R = -0.19$
Node strength	$p = 1$, $R = 0.0002$	$p = 0.058$, $R = -0.2$

Table 2 $F1$-score, accuracy, precision and recall for a classifier trained on DFA exponent values in the right frontal region in the alpha range showing statistically significant correlation with the result of performing Raven's progressive matrices

$F1$-score	0.8
Accuracy	0.76
Precision	0.75
Recall	0.85
p-value [Acc >NIR]	0.01

3.4 Results of classification

To validate the identified biomarkers, a classifier was trained to classify subjects according to their success in performing Raven's progressive matrices. For this purpose, subjects were divided into two classes based on the median value of the score assigned after passing the Raven's progressive matrices. The classifier was trained on the DFA exponent values in the alpha range, showing a correlation with the result of passing the Raven's progressive matrices (Fig. 1B), as well as with the network metrics.

The classification results are shown in Table 2. It can be seen that the classifier has quite high accuracy, with the $F1$ metric reaching a score of 0.8, which makes it a promising candidate for practical applications.

To assess the statistical significance of the achieved classification accuracy, a binomial test was performed to determine whether it exceeds the NIR (No Information Rate). NIR represents the baseline accuracy obtained by simply assigning all test samples to the most common class in the dataset. The p-value [Acc > NIR] presented in Table 2 indicates the probability of obtaining the same or higher accuracy than a random model, provided that the model predictions are essentially random (i.e., equivalent to NIR). This p-value corresponds to a hypothesis test in which H_0 states that model accuracy is not significantly better than NIR, and H_1 states that model accuracy is significantly better than NIR. Statistical testing was performed using standard tools for assessing model quality available in the caret library for R [43].

The classification results are visualised in Fig. 5 using the ROC curve. The figure shows the mean value for all folds as well as the standard deviation.

4 Discussion

Our study revealed a key role of alpha-band neurodynamics in supporting fluid intelligence in children aged 8–14 years, as measured by Raven's Progressive Matrices (RPM). We found that individual differences in RPM performance correlate both with the structure of long-range temporal correlations (calculated by detrended fluctuation analysis, DFA) in the right frontal region and with the topology of functional connectivity (phase-locking value, PLV). Notably, these two families of neurophysiological markers demonstrated an interrelationship: higher DFA values in the right frontal cortex were associated with a lower clustering coefficient in the "negative" network, that is, the network whose connections negatively correlate with success on the Raven's test. These findings suggest that efficient cognitive performance in children is linked not to isolated characteristics of brain activity, but to their coordinated interaction.

Linkenkaer-Hansen and colleagues first demonstrated that amplitude fluctuations of ongoing alpha oscillations exhibit power-law scaling with long-range temporal correlations extending over thousands of cycles which is a sign of critical-state dynamics that optimizes neural networks for rapid reorganization during cognitive demands [44]. DFA quantifies precisely this temporal persistence of amplitude modulation, providing a window into the system's proximity to criticality [20]. Critically, DFA reflects a dimension of neural dynamics fundamentally distinct from traditional spectral power measures. Multiple studies have confirmed the statistical independence between DFA scaling exponents and oscillation amplitude [44, 45], establishing DFA as a complementary biomarker that captures the temporal stability of network interactions rather than their instantaneous intensity. This independence was

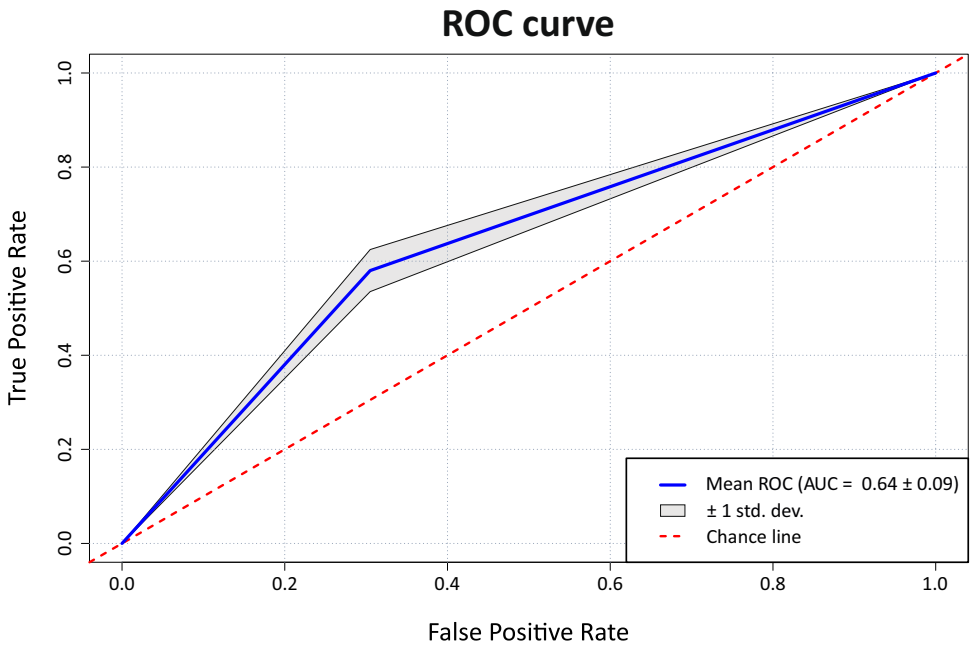


Fig. 5 ROC curve for SVM classifier

confirmed in [46], where it was demonstrated that DFA, power spectral density, and coherence provide mutually informative perspectives on cognitive workload, where DFA specifically characterizes the duration and persistence of information flow that spectral metrics cannot capture.

The reliability of DFA as an individual trait marker is well known. Nikulin and Brismar demonstrated high test-retest reliability of DFA exponents across days, particularly in resting-state conditions, confirming that scaling exponents reflect stable, subject-specific properties of neural dynamics rather than transient fluctuations [45]. This stability underlies the usefulness of DFA as a biomarker for cognitive assessment. In our prior work with a subset of this cohort (children aged 8–10 years), we established that frontal alpha-range DFA exponents significantly correlate with RPM performance and can serve as an objective neurophysiological predictor of intellectual capacity [47]. Subsequent validation using machine learning approaches confirmed that DFA-based features alone achieve robust classification accuracy in distinguishing children with high and low scores in intelligence tests [48], which enhances the potential of DFA as a quantitative biomarker for cognitive development assessment.

Our findings are consistent with current perspectives on the alpha rhythm as an active mechanism of top-down control. According to the hypothesis by Klimesch and colleagues, alpha synchronization reflects not a passive resting state but active inhibitory processes aimed at suppressing irrelevant information [49]. Jensen and Mazaheri extended this idea into the concept of "Gating by Inhibition," proposing that alpha activity functionally blocks task-irrelevant pathways, directing information flow toward relevant areas [9]. Within the context of our study, the "negative" network, whose connections are negatively correlated with intelligence, may represent a map of such functional inhibition. It is important to note that the negative correlation between frontal alpha DFA and this network's clustering coefficient suggests that children with higher intelligence demonstrate not only stronger temporal persistence in frontal alpha dynamics but also a less clustered, potentially more optimized architecture of inhibitory control networks. In [50], it was shown that preparatory alpha suppression in sensory regions is driven by frontal modulators. Our results extend this by showing that even at rest, the temporal organization of frontal alpha dynamics predicts the efficiency of large-scale inhibitory network topology.

The importance of alpha dynamics in childhood cognition finds support in developmental literature. Han and colleagues reported that resting-state upper alpha power (10–13 Hz) positively correlates with working memory capacity in children aged 3–9 years, particularly in right central regions [8]. Guntekin and colleagues also showed that successful memory encoding in 6–7-year-old children is accompanied by alpha enhancement, which contrasts with the suppression of alpha rhythm in adults, suggesting that alpha rhythms play a more pronounced role in active maintenance of representations during development before cognitive processes become fully automatized [51]. Our findings extend this developmental perspective by demonstrating that not merely alpha power but its temporal organization serves as a sensitive marker of intellectual capacity during middle childhood.

According to the pulsed-inhibition framework proposed by Mathewson and colleagues, the alpha rhythm creates alternating microstates of excitability, and the phase of alpha oscillations at the moment of stimulus presentation critically influences its perception [52]. DFA, by measuring long-range correlations in the amplitude envelope, characterizes the temporal persistence of this rhythmic pattern. Importantly, the stability of amplitude modulation is inextricably linked to phase organization [53]. Thus, increased DFA values in the right frontal cortex may reflect

not only the stability of amplitude dynamics but also a more predictable phase organization of the alpha rhythm, which is a necessary condition for effective top-down control and the temporal coordination of fronto-parietal networks.

The emphasis on the right frontal cortex and fronto-parietal connections aligns with research linking these areas to fluid intelligence. Specifically, the study by Penhale and colleagues directly associates age-related changes in alpha/beta activity with the function of the right prefrontal and parietal regions within the P-FIT model of intelligence [54]. The authors demonstrated that changes in functional connectivity between parietal and frontal regions play a key role in supporting fluid intelligence in adults. Our data extend these findings to childhood, showing that individual differences in intelligence at this developmental stage are already linked to the organization of this very network.

The negative correlation between DFA and clustering coefficient in the "negative" network resonates with findings from network neuroscience. Recent work has shown that non-verbal intelligence is negatively correlated with network segregation measures (clustering coefficient and modularity) in the alpha band, suggesting that higher cognitive performance is associated with more integrated network architecture [55]. In other study, it was found that successful visual-spatial thinking is associated with negative global brain connectivity in the primary visual cortex and precuneus, interpreted as functional segregation necessary for efficient feature processing [56]. Our results complement these findings by showing that the temporal stability of alpha oscillations is associated with a decrease in clustering in networks, which potentially affects task performance.

The "positive" network in our study, characterized by frontal-occipital connections, may reflect the functional architecture supporting cognitive control. This interpretation is supported by studies showing that fluid intelligence is associated with changes in functional connections in the fronto-parietal network caused by working memory [57]. In [58], causal evidence was presented that damage to the fronto-parietal network disrupts the modulation of alpha-band phase synchronization and cognitive flexibility, emphasizing the need for this network for dynamic control of synchronization over long distances.

In addition, it is worth noting the limitations of this study. Firstly, the cross-sectional design, which covers a wide age range from 8 to 14 years, does not allow tracing the individual development trajectories of the identified neurophysiological markers. To determine whether the observed correlations between the dynamics of the alpha range and fluid intelligence reflect stable personal characteristics, longitudinal studies are needed. Secondly, although the use of resting EEG provides valuable information about the internal architecture of the brain, it remains unclear to what extent the identified patterns of DFA and connectivity predict cognitive productivity in an active environment. Thirdly, a relatively homogeneous sample made up of students from the same school limits the possibility of generalizing conclusions to broader populations.

5 Conclusion

The present study demonstrates that individual differences in fluid intelligence in children aged 8–14 years are associated with both long-range temporal correlations in the right frontal area and the topology of functional networks in the alpha band. These two classes of neurophysiological markers were found to be interrelated: higher DFA values correlated with a lower clustering coefficient in the network whose connections were negatively associated with Raven's test performance. These findings suggest that effective cognitive functioning in childhood is determined by the coordinated interaction between the temporal stability of alpha oscillations and the topological organization of functional networks.

The high classification accuracy (76%, $F1$-score = 0.8) based on the identified markers supports their potential as objective biomarkers of cognitive development. Despite limitations related to the cross-sectional design and sample homogeneity, the obtained results open perspectives for early identification of children at risk of cognitive difficulties and for the development of personalized intervention programs.

Acknowledgements This work is supported from the Russian Science Foundation (project 24-71-00106).

Data Availability The dataset presented in this study can be obtained on request.

References

1. S. Greiff, S. Wüstenberg, T. Goetz, M.-P. Vainikainen, J. Hautamäki, M.H. Bornstein, A longitudinal study of higher-order thinking skills: working memory and fluid reasoning in childhood enhance complex problem solving in adolescence. Front. Psychol. **6**, 1060 (2015)
2. P. Kent, Fluid intelligence: a brief history. Appl. Neuropsychol. Child **6**(3), 193–203 (2017)
3. E. Ferrer, E.D. O'Hare, S.A. Bunge, Fluid reasoning and the developing brain. Front. Neurosci. **3**, 481 (2009)

4. S.A. Brouwers, F.J. Vijver, D.A. Van Hemert, Variation in raven's progressive matrices scores across time and place. Learn. Individ. Differ. **19**(3), 330–338 (2009)
5. M. Orsoni, M. Spinoso, S. Garofalo, N. Mazzoni, S. Giovagnoli, D. De Chiusole, P. Anselmi, A. Bacherini, I. Pierluigi, L. Stefanutti et al., Bayesian networks to evaluate and test the raven s colored progressive matrices. Intelligence **113**, 101964 (2025)
6. N. Priyadarshani, S. Senarath, Enhancing the identification of gifted students in schools in sri lanka: a dual framework utilizing teacher and parent nominations along with raven's matrices. Muallim J. Soc. Sci. Humanit. **9**(4), 84–97 (2025)
7. E. Ünsal, R. Duygun, İ Yemeniciler, E. Bingöl, Ö. Ceran, B. Güntekin, From infancy to childhood: a comprehensive review of event-and task-related brain oscillations. Brain Sci. **14**(8), 837 (2024)
8. J. Han, Z. Yang, M. Ma, L. Liang, X. Li, Developmental changes in spontaneous electrical activity from early to middle childhood and their relation to short-term working memory ability. Int. J. Psychophysiol. **215**, 113238 (2025)
9. O. Jensen, A. Mazaheri, Shaping functional architecture by oscillatory alpha activity: gating by inhibition. Front. Hum. Neurosci. **4**, 186 (2010)
10. A. Kuc, V. Maksimenko, A. Savosenkov, N. Grigorev, V. Grubov, A. Badarin, V. Kazantsev, S. Gordleeva, A. Hramov, Studying perceptual bias in favor of the from-above necker cube perspective in a goal-directed behavior. Front. Psychol. **14**, 1160605 (2023)
11. A. Kuc, V.V. Grubov, V.A. Maksimenko, N. Shusharina, A.N. Pisarchik, A.E. Hramov, Sensor-level wavelet analysis reveals eeg biomarkers of perceptual decision-making. Sensors **21**(7), 2461 (2021)
12. Y. Zeng, P. Sauseng, A. Alamia, Alpha traveling waves during working memory: disentangling bottom-up gating and top-down gain control. J. Neurosci. **44**(50) (2024)
13. C.-A. Tu, T. Parviainen, J.A. Hämäläinen, Y.-F. Hsu, Alpha oscillations protect auditory working memory against distractors in the encoding phase. Neuropsychologia **207**, 109058 (2025)
14. A.K. Barbey, Network neuroscience theory of human intelligence. Trends Cogn. Sci. **22**(1), 8–20 (2018)
15. K.J. Friston, Functional and effective connectivity: a review. Brain Connect. **1**(1), 13–36 (2011)
16. S. Aydore, D. Pantazis, R.M. Leahy, A note on the phase locking value and its properties. Neuroimage **74**, 231–244 (2013)
17. M.P. Van Den Heuvel, C.J. Stam, R.S. Kahn, H.E.H. Pol, Efficiency of functional brain networks and intellectual performance. J. Neurosci. **29**(23), 7619–7624 (2009)
18. A. Safron, V. Klimaj, I. Hipólito, On the importance of being flexible: dynamic brain networks and their potential functional significances. Front. Syst. Neurosci. **15**, 688424 (2022)
19. K.B. Hengen, W.L. Shew, Is criticality a unified setpoint of brain function? Neuron **113**(16), 2582–2598 (2025)
20. R. Hardstone, S.-S. Poil, G. Schiavone, R. Jansen, V.V. Nikulin, H.D. Mansvelder, K. Linkenkaer-Hansen, Detrended fluctuation analysis: a scale-free view on neuronal oscillations. Front. Physiol. **3**, 23105 (2012)
21. M.N. Perquin, M.K. Vugt, C. Hedge, A. Bompas, Temporal structure in sensorimotor variability: a stable trait, but what for? Comput. Brain Behav. **6**(3), 400–437 (2023)
22. J.R. Gray, C.F. Chabris, T.S. Braver, Neural mechanisms of general fluid intelligence. Nat. Neurosci. **6**(3), 316–322 (2003)
23. J.L. Horn, R.B. Cattell, Refinement and test of the theory of fluid and crystallized general intelligences. J. Educ. Psychol. **57**(5), 253 (1966)
24. R.B. Cattell, Theory of fluid and crystallized intelligence: a critical experiment. J. Educ. Psychol. **54**(1), 1 (1963)
25. S. Greiff, J.C. Neubert, On the relation of complex problem solving, personality, fluid intelligence, and academic achievement. Learn. Individ. Differ. **36**, 37–48 (2014)
26. L.S. Colzato, N.C. Van Wouwe, T.J. Lavender, B. Hommel, Intelligence and cognitive flexibility: fluid intelligence correlates with feature unbinding across perception and action. Psychon. Bull. Rev. **13**, 1043–1048 (2006)
27. V.V. Grubov, M.V. Khramova, S. Goman, A.A. Badarin, S.A. Kurkin, D.A. Andrikov, E. Pitsik, V. Antipov, E. Petushok, N. Brusinskii et al., Open-loop neuroadaptive system for enhancing student s cognitive abilities in learning. IEEE Access **12** (2024)
28. G.E. Chatrian, E. Lettich, P.L. Nelson, Ten percent electrode system for topographic studies of spontaneous and evoked eeg activities. Am. J. EEG Technol. **25**(2), 83–92 (1985)
29. J. Iriarte, E. Urrestarazu, M. Valencia, M. Alegre, A. Malanda, C. Viteri, J. Artieda, Independent component analysis as a tool to eliminate artifacts in eeg: a quantitative study. J. Clin. Neurophysiol. **20**(4), 249–257 (2003)
30. R. Oostenveld, P. Fries, E. Maris, J.-M. Schoffelen, Fieldtrip: open source software for advanced analysis of meg, eeg, and invasive electrophysiological data. Comput. Intell. Neurosci. **2011**(1), 156869 (2011)
31. A. Badarin, A. Andreev, V. Klinshov, V. Antipov, A.E. Hramov, Hidden data recovery using reservoir computing: adaptive network model and experimental brain signals. Chaos Interdiscip. J. Nonlinear Sci. **34**(10) (2024)
32. C.-K. Peng, S. Havlin, H.E. Stanley, A.L. Goldberger, Quantification of scaling exponents and crossover phenomena in nonstationary heartbeat time series. Chaos Interdiscip. J. Nonlinear Sci. **5**(1), 82–87 (1995)
33. V.V. Grubov, A.K. Kuc, S.A. Kurkin, D.A. Andrikov, N. Utyashev, V.A. Maksimenko, O.E. Karpov, A.E. Hramov, Harnessing long-range temporal correlations for advanced epilepsy classification. PRX Life **3**(1), 013005 (2025)
34. C.-K. Peng, S.V. Buldyrev, S. Havlin, M. Simons, H.E. Stanley, A.L. Goldberger, Mosaic organization of dna nucleotides. Phys. Rev. E **49**(2), 1685 (1994)
35. J. Freschl, L. Al Azizi, L. Balboa, Z. Kaldy, E. Blaser, The development of peak alpha frequency from infancy to adolescence and its role in visual temporal processing: A meta-analysis. Dev. Cogn. Neurosci. **57**, 101146 (2022)

36. R.M. Bryce, K.B. Sprague, Revisiting detrended fluctuation analysis. Sci. Rep. **2**(1), 315 (2012)
37. E. Maris, R. Oostenveld, Nonparametric statistical testing of eeg-and meg-data. J. Neurosci. Methods **164**(1), 177–190 (2007)
38. A.A. Badarin, V.M. Antipov, V.V. Grubov, A.V. Andreev, E.N. Pitsik, S.A. Kurkin, A.E. Hramov, Brain compensatory mechanisms during the prolonged cognitive task: fnirs and eye-tracking study. IEEE Trans. Cogn. Dev. Syst. **17**(2), 303–314 (2024)
39. J.-P. Lachaux, E. Rodriguez, J. Martinerie, F.J. Varela, Measuring phase synchrony in brain signals. Hum. Brain Mapp. **8**(4), 194–208 (1999)
40. E. Gysels, P. Celka, Phase synchronization for the recognition of mental tasks in a brain-computer interface. IEEE Trans. Neural Syst. Rehabil. Eng. **12**(4), 406–415 (2004)
41. X. Shen, E.S. Finn, D. Scheinost, M.D. Rosenberg, M.M. Chun, X. Papademetris, R.T. Constable, Using connectome-based predictive modeling to predict individual behavior from brain connectivity. Nat. Protoc. **12**(3), 506–518 (2017)
42. C. Goutte,E. Gaussier, A probabilistic interpretation of precision, recall and f-score, with implication for evaluation. In *European Conference on Information Retrieval*, vol. 3408 (Springer, Berlin, 2005), pp. 345–359
43. M. Kuhn, Building predictive models in r using the caret package. J. Stat. Softw. **28**, 1–26 (2008)
44. K. Linkenkaer-Hansen, V.V. Nikouline, J.M. Palva, R.J. Ilmoniemi, Long-range temporal correlations and scaling behavior in human brain oscillations. J. Neurosci. **21**(4), 1370–1377 (2001)
45. V.V. Nikulin, T. Brismar, Long-range temporal correlations in alpha and beta oscillations: effect of arousal level and test-retest reliability. Clin. Neurophysiol. **115**(8), 1896–1908 (2004)
46. I. Seleznov, I. Zyma, K. Kiyono, S. Tukaev, A. Popov, M. Chernykh, O. Shpenkov, Detrended fluctuation, coherence, and spectral power analysis of activation rearrangement in eeg dynamics during cognitive workload. Front. Hum. Neurosci. **13**, 270 (2019)
47. A. Kuc, V. Grubov, A. Badarin, Using long-range temporal correlations in the brain to predict intellectual development in children. In *2024 8th Scientific School Dynamics of Complex Networks and Their Applications (DCNA) . IEEE* (2024), pp. 142–144
48. A.K. Kuc, Frontal long-range temporal correlations as a predictor of child s iq test performance using machine learning approach. Eur. Phys. J. Spec. Top. **234**(15), 4109–4125 (2025)
49. W. Klimesch, P. Sauseng, S. Hanslmayr, Eeg alpha oscillations: the inhibition-timing hypothesis. Brain Res. Rev. **53**(1), 63–88 (2007)
50. K.E. Mathewson, D.M. Beck, T. Ro, E.L. Maclin, K.A. Low, M. Fabiani, G. Gratton, Dynamics of alpha control: preparatory suppression of posterior alpha oscillations by frontal modulators revealed with combined eeg and event-related optical signal. J. Cogn. Neurosci. **26**(10), 2400–2415 (2014)
51. B. Güntekin, H. Uzunlar, P. Çalışoğlu, F. Eroğlu-Ada, E. Yıldırım, T. Aktürk, E. Atay, Ö. Ceran, Theta and alpha oscillatory responses differentiate between six-to seven-year-old children and adults during successful visual and auditory memory encoding. Brain Res. **1747**, 147042 (2020)
52. K.E. Mathewson, A. Lleras, D.M. Beck, M. Fabiani, T. Ro, G. Gratton, Pulsed out of awareness: Eeg alpha oscillations represent a pulsed-inhibition of ongoing cortical processing. Front. Psychol. **2**, 99 (2011)
53. S. Palva, New vistas for α-frequency band oscillations. Trends Neurosci. **30**(4), 553 (2003)
54. S.H. Penhale, Y. Arif, M. Schantell, H.J. Johnson, M.P. Willett, H.J. Okelberry, C.E. Meehan, E. Heinrichs-Graham, T.W. Wilson, Healthy aging alters the oscillatory dynamics and fronto-parietal connectivity serving fluid intelligence. Hum. Brain Mapp. **45**(3), 26591 (2024)
55. I. Feklicheva, I. Zakharov, N. Chipeeva, E. Maslennikova, S. Korobova, T. Adamovich, V. Ismatullina, S. Malykh, Assessing the relationship between verbal and nonverbal cognitive abilities using resting-state eeg functional connectivity. Brain Sci. **11**(1), 94 (2021)
56. Z. Chen, A. De Beuckelaer, X. Wang, J. Liu, Distinct neural substrates of visuospatial and verbal-analytic reasoning as assessed by raven s advanced progressive matrices. Sci. Rep. **7**(1), 16230 (2017)
57. H. Takeuchi, Y. Taki, R. Nouchi, R. Yokoyama, Y. Kotozaki, S. Nakagawa, A. Sekiguchi, K. Iizuka, S. Hanawa, T. Araki et al., General intelligence is associated with working memory-related functional connectivity change: evidence from a large-sample study. Brain Connect. **11**(2), 89–102 (2021)
58. S. Sadaghiani, P.L. Dombert, M. Løvstad, I. Funderud, T.R. Meling, T. Endestad, R.T. Knight, A.-K. Solbakk, M. D Esposito, Lesions to the fronto-parietal network impact alpha-band phase synchrony and cognitive control. Cereb. Cortex **29**(10), 4143–4153 (2019)

Springer Nature or its licensor (e.g. a society or other partner) holds exclusive rights to this article under a publishing agreement with the author(s) or other rightsholder(s); author self-archiving of the accepted manuscript version of this article is solely governed by the terms of such publishing agreement and applicable law.